frontiers
in Marine Science

Utilization of Soot and ^{210}Po-^{210}Pb Disequilibria to Constrain Particulate Organic Carbon Fluxes in the Northeastern South China Sea

Weifeng Yang[1,2]*, Xiufeng Zhao[1,2], Laodong Guo[3], Bangqin Huang[1,4], Min Chen[2], Ziming Fang[5], Xiao Zhang[2] and Yusheng Qiu[2]

[1] State Key Laboratory of Marine Environmental Science, Xiamen, China, [2] College of Ocean and Earth Sciences, Xiamen University, Xiamen, China, [3] School of Freshwater Sciences, University of Wisconsin-Milwaukee, Milwaukee, WI, United States, [4] College of the Environment and Ecology, Xiamen University, Xiamen, China, [5] Department of Ocean Science, The Hong Kong University of Science and Technology, Kowloon, Hong Kong SAR, China

Black carbon (BC) is believed to be refractory and thus affects the timescale of organic carbon conversion into CO_2 and the magnitude of the sink of CO_2. However, the fate of BC in the oceans remains poorly understood. Here, ^{210}Po and ^{210}Pb were measured to examine the export of soot in the northeastern South China Sea (SCS). Concentrations of soot decreased from 0.141 ± 0.021 μmol-C L^{-1} (mean ± SD) in the mixed layer (0–30 m) to 0.087 μmol-C L^{-1} at the euphotic base (150 m) due to potential photodegradation within the euphotic zone. In the twilight zone, however, the soot showed an increasing pattern along with the total particulate matter and total particulate organic carbon (POC) contents, corresponding to additions from the shelf/slope sediment resuspension through lateral transport. Using the deficits of ^{210}Po, the export flux of soot from the euphotic zone was calculated to be 0.172 ± 0.016 mmol-C m^{-2} d^{-1} and increased with depth. Assuming that the soot is entirely refractory below the euphotic zone, the sediment-derived soot fluxes were estimated based on the increase in soot fluxes relative to the base of the euphotic zone, with values varying from 0.149 ± 0.030 to 0.96 ± 0.10 μmol-C L^{-1}. This indicates that sediment resuspension is an important source of soot to the ocean interior in the SCS. Coupling the sediment-derived soot and ^{210}Po-derived POC fluxes gave rise to a Martin Curve-like flux attenuation of local euphotic zone-derived POC in the twilight zone with b value of 0.70 ± 0.01. These results suggest that soot could be useful for constraining *in situ* POC fluxes and their transport.

Keywords: soot, polonium, South China Sea, twilight zone, black carbon, biological pump efficiency

INTRODUCTION

Black carbon (BC) is the product of incomplete combustion of biomass and fossil fuels (Goldberg, 1985). In the atmosphere, BC has a strong ability to absorb solar radiation (Jacobson, 2001), and thus it has been listed as the second forcing factor in driving the global change following CO_2 (Ramanathan and Carmichael, 2008). Owing to its chemical- (except photolysis) and bio-resistant

nature, BC represents the refractory carbon pool on the earth. Previous studies have shown that most of the BC can persist for hundreds to thousands of years either in the soil (Goldberg, 1985; Singh et al., 2012) or in seawater (Ziolkowski and Druffel, 2010; Coppola and Druffel, 2016). Thus, BC is a long-term CO_2 sink (Coppola et al., 2014). Understanding the fate of BC would increase our knowledge about the role of BC in the global carbon cycle and climate change.

Over the past years, a line of studies indicated that a large amount of BC gets into the oceans *via* atmospheric deposition (Bao et al., 2017) and river discharge (Wang et al., 2016; Jones et al., 2020). For example, the annual particulate BC (PBC) input from the river discharge was 17–37 Tg (Coppola et al., 2018). Around 34 ± 26% of biomass-generated BC (40–215 Tg yr^{-1}, including dissolved BC, i.e., DBC and PBC) gets into the oceans *via* river discharge (Jones et al., 2020). These reports indicate that the ocean is an important reservoir of BC (Masiello and Druffel, 1998; Fang et al., 2018). With an increase in BC emissions from the increase in both fossil fuel combustion and fires emissions, the riverine BC is expected to increase the refractory carbon pool in abyssal oceans (Cheng et al., 2008; Dittmar et al., 2012). However, the cycling of BC in marine environments remains enigmatic with available data.

Based on radiocarbon measurements, BC in deep oceans has a ^{14}C-age ranging from thousands to tens of thousands of years (Ziolkowski and Druffel, 2010; Coppola et al., 2014; Coppola and Druffel, 2016). However, the global riverine discharge could renew the oceanic BC pool within hundreds of years (Wagner et al., 2018). These results indicate that there must be a large amount of BC being removed after getting into the marine environment. Three recent reports suggested that δ^{13}C signal, ^{14}C age, and DBC spatial pattern support a significant removal of riverine BC in coastal seas (Wagner et al., 2019; Qi et al., 2020; Fang et al., 2021). Available studies have shown that two pathways are responsible for the removal of BC in the ocean. One is photochemical degradation, especially for the condensed aromatic molecular structures (Ziolkowski and Druffel, 2010). This process is proved by *in situ* seawater incubation experiments on DBC (Stubbins et al., 2012; Ward et al., 2014) and the decrease in DBC with depth in the euphotic zone (Fang et al., 2017). The other removal mechanism is the sinking of PBC, which has been reported in different marine environments, such as the Gulf of Maine (Flores-Cervantes et al., 2009), the western Arctic, and Subarctic Ocean (Fang et al., 2016), and Jiaozhou Bay (Feng et al., 2021). Yet, future research is needed to better understand the fate of BC in the ocean, especially regarding the quantification of the magnitude of the removal of BC from the water column.

Since the riverine BC is first discharged into the marginal seas, it is crucial to assess the fate and transport pathways of BC in the marginal seas and thus the cycling of BC in the ocean (Yang and Guo, 2014; Fang et al., 2017). As an important removal process of BC, knowledge about the sinking of PBC would provide insights into the role of BC in transporting carbon from the surface ocean to the deep ocean. As a refractory and photolabile fraction of BC (Stubbins et al., 2012; Fang et al., 2017), the soot was found to distribute widely in shelf

sediments (Lohmann et al., 2009; Yang and Guo, 2018). Thus, it is probable that shelf/slope might be of importance for assessing the removal of soot in marine environments. Additionally, soot has been reported as a fraction of particulate organic carbon (POC; Flores-Cervantes et al., 2009; Yang and Guo, 2014; Fang et al., 2016). Investigations on soot, including its abundance and export, should improve our understanding of POC dynamics in the oceans.

The South China Sea (SCS) is the largest marginal sea in the western Pacific Ocean (Chen et al., 2001), which is surrounded by the BC emission hotspots of the world in Southeast Asia countries (Hu et al., 2016). Asia emits more than 1/3 of the global BC (Jurado et al., 2008; Bond et al., 2013). With the prevailing of the Asian monsoons (Wang et al., 2014; Zhang et al., 2016), the SCS is expected to be an important BC reservoir. In this study, the soot was measured along with ^{210}Po and ^{210}Pb in the northeastern SCS. Our objectives are to (i) examine the abundance and vertical distribution of soot on the slope of the northeastern SCS; (ii) evaluate the export of soot from the euphotic zone to the mesopelagic water and the fate of soot in the SCS; and (iii) explore the potential application of soot to constrain the POC flux in the marginal sea.
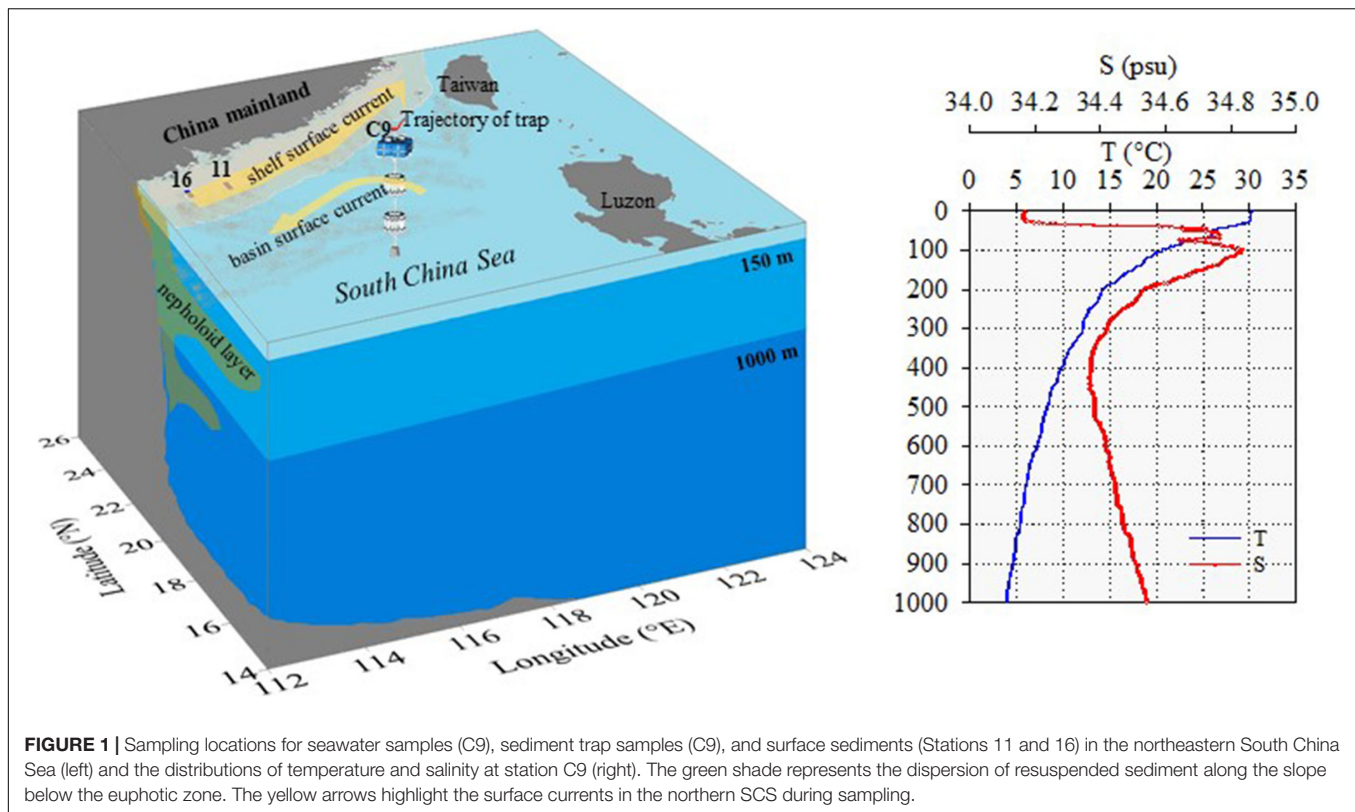
MATERIALS AND METHODS

Study Area
The main current on the northern SCS shelf flows northeastward and the surface current flows southwestward in the northern basin during summer. Internal solitary waves often introduce the bottom nepheloid layer (BNL) on the northern shelf (Zhang et al., 2014) and the intermediate nepheloid layer (INL) on the slope (Jia et al., 2019). Both the BNLs and INLs result in higher particulate matter concentrations in the mesopelagic layer than the euphotic zone in the SCS (Ma et al., 2017; Zhang et al., 2019) and a large amount of shelf-derived sedimentary matter to the basin (Shih et al., 2019). Particles in the widely extended nepheloid layer over the shelf-slope area of the northern SCS are mainly from sediment resuspension (Zhang et al., 2014; Jia et al., 2019). Owing to the variability in the hydrodynamic conditions, the nepheloid layer also showed significant spatiotemporal variability as observed at different depths during different cruises (Zhang et al., 2019). The C9 station is located on the northeastern SCS slope with a depth of 1,369 m (**Figure 1**). Salinity distributions show complex variability in the upper 100 m (**Figure 1**). The mixed layer of about 30 m (**Figure 1**) is consistent with previous observations during summer in the north SCS (Cai et al., 2015), corresponding to the shallow stratification in summer.

Sampling
Seawater samples at different depths were collected at station C9 (**Figure 1**) using Niskin bottles attached to a conductivity, temperature and depth (CTD)-rosette system aboard the *R/V Yanping* for the measurements of ^{210}Po, ^{210}Pb, soot, and POC on August 8, 2016. In addition, a floating sediment trap having

FIGURE 1 | Sampling locations for seawater samples (C9), sediment trap samples (C9), and surface sediments (Stations 11 and 16) in the northeastern South China Sea (left) and the distributions of temperature and salinity at station C9 (right). The green shade represents the dispersion of resuspended sediment along the slope below the euphotic zone. The yellow arrows highlight the surface currents in the northern SCS during sampling.

a cylindrical cup with an internal diameter of 95 mm was deployed for 72 h (August 9–12, 2016) to collect sinking particles at 50 and 200 m for ^{210}Po and POC measurements. The cup was filled with brine with a salinity of 52 psu, prepared by freezing filtered SCS surface water (0.2 μm pore size). Mercury bichloride was added as a biocide. Owing to limited particles from the sediment trap, the soot was not measured. Surface sediments were sampled using a box core sampler at two stations (Stations 11 and 16) on the northern SCS shelf on March 28, 2014 (**Figure 1**) for the measurements of soot and sedimentary organic carbon (SOC).

^{210}Po and ^{210}Pb Analyses

For the measurements of ^{210}Po and ^{210}Pb, 10 L of seawater from each depth was filtered through a polycarbonate membrane (Isopore^{TM}) with 0.4 μm pore size to separate >0.4 μm particulate matter from dissolved phases. Analyses of ^{210}Po and ^{210}Pb in the <0.4 μm filtrate and >0.4 μm particulate samples were based on the widely used protocols (Church et al., 2012; Rigaud et al., 2013) and elaborated in our previous works (Yang et al., 2013; Ma et al., 2017), which would enable our results to compare with most of the published data. In brief, filtrate samples, after adding accurately known amounts of ^{209}Po and stable Pb (PbNO$_3$) as the chemical yields of ^{210}Po and ^{210}Pb isotopes, respectively, were kept for 24 h to reach the isotopic distribution equilibrium. Then, the samples were adjusted to pH = 8.0 with ammonium

hydroxide to form Fe(OH)$_3$ precipitate. The precipitate was allowed to settle overnight and collected *via* centrifugation and decanting the overlying water. Then, the precipitate was redissolved in 0.5 mol L^{-1} HCl solution. After adding ascorbic acid, hydroxylamine hydrochloride, and sodium citrate, Po isotopes including ^{209}Po and ^{210}Po were plated on a silver disk at 90°C for 4 h under stirring. The air-dried silver disk was counted using alpha-spectrometry (ORTEC). Particulate samples were digested with mixed HNO$_3$-HClO$_4$-HF after adding ^{209}Po and stable Pb, evaporated and redissolved in 0.5 mol L^{-1} HCl solution. The plating of Po on the silver disk was the same as that for dissolved samples. ^{210}Pb was determined *via* ^{210}Po more than 1.5 years later after the first plating.

The sediment trap collected particles were filtered through a mesh with 1,000 μm pore size to remove swimmers and zooplankton. Then, one aliquot of the small particles was collected on a polycarbonate membrane for ^{210}Po and ^{210}Pb measurements, and the treatment was the same as the particulate fractions. The other aliquot was collected on a quartz microfiber filter (QMA) filter for POC measurements. The recoveries of ^{209}Po and stable Pb for dissolved samples varied from 84 to 94% and from 85 to 93%, respectively. They were more than 95% for particulate samples including trap samples. The counting errors were always <±8%. The uncertainties for all data presented in the study were propagated from the counting errors by incorporating detector backgrounds, reagent blanks,

and membrane blanks. The activities of ^{210}Po and ^{210}Pb were corrected back to the sampling time.

Total Particulate Matter Analysis

For the measurements of total particulate matter (i.e., TPM), along with soot, and POC, 30–48 L of seawater were collected from each depth except the 500 and 1,000 m depths, where only 5 L of seawater were available and were used for POC measurements. Particles were filtered onto a pre-combusted (at 450°C) QMA filter (Whatman^{TM}) and de-salted with Milli-Q water. Particulate samples were stored at −18°C. In the land laboratory, these filter samples were dried at 60°C to a constant weight to determine the TPM contents based on the difference in weight between blank filters and filters with TPM.

Particulate Organic Carbon and Soot Analyses

For the measurements of POC, the samples were fumigated using concentrated HCl to remove inorganic carbon. The total POC content (including soot and autochthonous POC) was measured on an aliquot of the filter sample using an elemental analyzer (Thermo Fisher Scientific, 1112). An aliquot of the filter samples was used to determine soot using the chemoThermal oxidation (CTO)-375 method (Gustafsson et al., 1997, 2001). This method has been proved to effectively quantify soot in sediment (Elmquist et al., 2004; Lohmann et al., 2009) and TPM samples (Yang and Guo, 2014; Fang et al., 2016). In brief, decarbonate filters were combusted at 375°C in the presence of air for 24 h to remove organic carbon except for soot. Then, the soot left on the filters was measured using the same elemental analyzer, as described for POC. The standard material used for POC and soot was international atomic energy agency (IAEA)-C8. The soot and SOC in sediments were measured using procedures described elsewhere (Yang and Guo, 2018). Briefly, the sediment was treated with HCl solution to eliminate carbonate and dried at 60°C. Then, an aliquot of samples was used to measure SOC. The other aliquot of sample was combusted using the same procedures as particulate samples to remove non-soot SOC in sediments. The soot was measured in a manner similar to particulate samples. The National Institute of Standards and Technology (NIST) standard 1941b was measured as samples to ensure data quality. The obtained soot and SOC contents in the standards agree well with previous reports on 1941b (e.g., Gustafsson et al., 2001; Louchouarn et al., 2007; Yang and Guo, 2014).

RESULTS

The soot concentrations measured along the water column varied from 0.064 to 0.165 µmol-C L^{-1} (**Table 1**) with an average of 0.110 ± 0.036 µmol-C L^{-1} (mean ± SD). Overall, the soot concentrations did not show an increase or decrease trend within the upper euphotic zone (0–75 m), though they had a fluctuation. From 75 m to the euphotic base (150 m), the soot contents showed a quick decline (**Figure 2A**). However, an increasing trend with depth in the soot contents was observed below 200 m, increasing from 0.064 µmol-C L^{-1} at 200 m to 0.090 µmol-C

TABLE 1 | Temperature, salinity, concentrations of soot and the total particulate organic carbon (POC), activity concentrations of dissolved ^{210}Po, ^{210}Pb, and particulate ^{210}Po, ^{210}Pb.

| Station	Depth	T	S	POC	Soot	^{210}Po$_D$	^{210}Po$_P$	^{210}Po$_T$	^{210}Pb$_D$	^{210}Pb$_P$	^{210}Pb$_T$	^{210}Po/^{210}Pb Diss.	^{210}Po/^{210}Pb Part.	^{210}Po/^{210}Pb Total
	(m)	(°C)	(psu)	(µmol-C L^{-1})		(dpm 100L^{-1})								
C9	0	30.25	34.17	2.119	n.d.	6.21 ± 0.56	1.29 ± 0.12	7.5 ± 0.57	15.1 ± 1.1	1.93 ± 0.20	17.0 ± 1.1	0.41 ± 0.05	0.67 ± 0.09	0.44 ± 0.03
21.67°N	10	30.11	34.17	0.952	0.121	5.44 ± 0.48	1.12 ± 0.10	6.56 ± 0.49	15.2 ± 1.1	0.98 ± 0.11	16.2 ± 1.1	0.36 ± 0.04	1.14 ± 0.16	0.41 ± 0.03
117.95°E	30	29.76	34.21	1.492	0.151	6.19 ± 0.42	1.81 ± 0.14	8.00 ± 0.44	16.7 ± 1.2	1.00 ± 0.12	17.7 ± 1.2	0.37 ± 0.04	1.81 ± 0.26	0.45 ± 0.03
2016-8-9	50	25.95	34.67	1.019	0.124	9.22 ± 0.68	2.32 ± 0.18	11.55 ± 0.70	15.6 ± 1.1	0.98 ± 0.14	16.6 ± 1.1	0.59 ± 0.06	2.38 ± 0.38	0.69 ± 0.05
	75	23.98	34.66	4.719	0.165	8.16 ± 0.66	2.51 ± 0.19	10.67 ± 0.69	18.8 ± 1.4	0.47 ± 0.10	19.3 ± 1.4	0.43 ± 0.05	5.30 ± 1.16	0.55 ± 0.05
	100	20.64	34.84	3.557	0.123	7.18 ± 0.61	2.57 ± 0.20	9.75 ± 0.64	16.7 ± 1.3	0.90 ± 0.15	17.6 ± 1.3	0.43 ± 0.05	2.85 ± 0.51	0.55 ± 0.04
	150	17.59	34.72	3.090	0.087	5.81 ± 0.56	3.37 ± 0.25	9.18 ± 0.62	20.4 ± 1.6	0.56 ± 0.12	21.0 ± 1.6	0.28 ± 0.04	5.99 ± 1.39	0.44 ± 0.04
	200	14.21	34.53	1.396	0.064	7.01 ± 0.60	2.05 ± 0.16	9.06 ± 0.62	15.4 ± 1.2	0.91 ± 0.13	16.4 ± 1.2	0.45 ± 0.05	2.25 ± 0.36	0.55 ± 0.04
	300	12.11	34.42	1.111	0.066	5.92 ± 0.48	2.56 ± 0.19	8.47 ± 0.52	13.9 ± 1.0	0.98 ± 0.14	14.9 ± 1.1	0.43 ± 0.05	2.62 ± 0.43	0.57 ± 0.05
	500	8.31	34.38	1.095	n.d.	6.24 ± 0.54	2.05 ± 0.15	8.29 ± 0.56	16.3 ± 1.1	0.68 ± 0.09	17.0 ± 1.1	0.38 ± 0.04	3.02 ± 0.47	0.49 ± 0.04
	800	5.40	34.47	0.930	0.090	7.01 ± 0.59	2.70 ± 0.20	9.72 ± 0.62	18.5 ± 1.3	0.82 ± 0.13	19.3 ± 1.3	0.38 ± 0.04	3.29 ± 0.57	0.50 ± 0.04
	1000	3.94	34.54	1.566	n.d.	7.87 ± 0.65	2.02 ± 0.15	9.89 ± 0.67	18.5 ± 1.2	0.88 ± 0.11	19.3 ± 1.2	0.43 ± 0.04	2.30 ± 0.33	0.51 ± 0.04
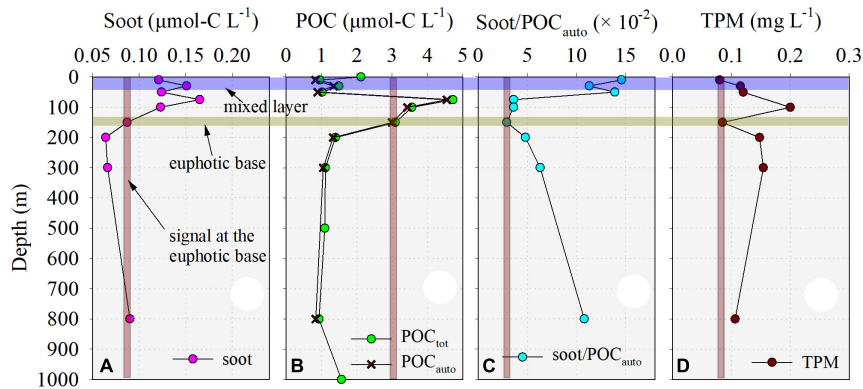
FIGURE 2 | Vertical distributions of soot **(A)**, total particulate organic carbon (POC) (i.e., POC_{tot}), autochthonous POC excluding soot (i.e., POC_{auto}) **(B)**, soot/POC_{auto} ratio **(C)**, and total particulate matter (TPM) **(D)** at station C9 on the slope of the northeastern South China Sea.

L^{-1} at 800 m (**Table 1**). The soot contents were 0.25 mg g^{-1} and 0.17 mg g^{-1} at Stations 11 and 16, respectively.

The total POC (POC_{tot}) concentrations in seawater samples varied from 0.93 to 4.72 µmol-C L^{-1}, averaging 1.92 ± 1.22 µmol-C L^{-1} (**Table 1**). Similar to soot, POC_{tot} showed little variation in the surface mixing layer (**Figure 2B**). The maximum of POC_{tot} concentration occurred at 75 m, corresponding to summer Chl-a maximum in the northern SCS (Cai et al., 2015). Within the lower euphotic zone, POC_{tot} showed a rapid decrease from 4.72 to 3.09 µmol-C L^{-1} (**Figure 2B**). Between 200 and 800 m, nearly constant POC_{tot} concentrations were observed, followed by an increase from 0.930 µmol-C L^{-1} at 800 m to 1.566 µmol-C L^{-1} at 1,000 m. The POC_{tot} contents on the trap-collected particulate matter were 9.12 µmol-C mg^{-1} and 3.66 µmol-C mg^{-1} at 50 and 200 m, respectively. The SOC contents in surface sediment were 2.54 mg g^{-1} and 1.66 mg g^{-1} at Stations 11 and 16, respectively.

The TPM concentrations varied from 0.08 to 0.20 mg L^{-1} with an average of 0.13 ± 0.04 mg L^{-1} (**Figure 2D**). In general, the vertical distribution of TPM followed that of POC in the euphotic zone, showing a dominant biological source of particulate matter. Notably, TPM and soot, both showed increases below the euphotic base (**Figure 2D**), with a TPM concentration of about 50% higher than the average at 150 m (0.09 mg L^{-1}).

The total ^{210}Po and ^{210}Pb activity concentrations varied from 6.56 to 11.55 dpm 100L^{-1} and from 14.89 to 21.00 dpm 100L^{-1}, respectively (**Table 1**), averaging 9.05 ± 1.39 dpm 100L^{-1} and 17.70 ± 1.72 dpm 100L^{-1}. The total ^{210}Po/^{210}Pb ratio ranged from 0.40 to 0.69, pointing to obvious deficits of ^{210}Po with respect to ^{210}Pb in the study area. Our results are consistent with those previously reported deficits of ^{210}Po for both the euphotic zone (Yang et al., 2009; Wei et al., 2011) and the mesopelagic water in the SCS (Wei et al., 2014; Ma et al., 2017). Although the Fe(OH)$_3$ coprecipitation method may lead to artificially low ^{210}Po concentrations, hence overestimating ^{210}Po deficits relative to ^{210}Pb (i.e., overestimating ^{210}Po fluxes) (Roca-Martí et al., 2021), the increases with the depth of soot, TPM, and POC_{tot} concentrations (**Figure 2**) indicate that the ^{210}Po deficits in the study site are clearly impacted by sediment-derived particulate

matter in the mesopelagic waters. The ^{210}Po activities on trap-collected particles were 0.160 dpm mg^{-1} and 0.056 dpm mg^{-1} at 50 and 200 m, respectively. The ^{210}Pb activities were somewhat lower than ^{210}Po with the values of 0.035 dpm mg^{-1} and 0.045 dpm mg^{-1}, respectively, corresponding to their difference in particle reactivity between ^{210}Po and ^{210}Pb.

DISCUSSION

Abundance and Distribution of Soot in the Northeastern South China Sea

To date, only limited soot data are available for seawater. As reported in previous studies, the soot concentrations varied from 0.004 to 0.233 µmol-C L^{-1} in the upper 60 m water column in the northern Gulf of Mexico (Yang and Guo, 2014), and from 0.008 to 0.080 µmol-C L^{-1} in surface waters of the Bering Shelf and Chukchi Sea (Fang et al., 2016). On average, the soot concentration in the euphotic zone of the SCS (avg. 0.129 ± 0.027 µmol-C L^{-1}, **Table 1**) was higher than both the Gulf of Mexico (avg. 0.050 ± 0.070 µmol-C L^{-1}, n = 14) (Yang and Guo, 2014) and the western Arctic and Subarctic Oceans (avg. 0.027 ± 0.020 µmol-C L^{-1}, n = 18) (Fang et al., 2016). High soot concentration average of 0.39 ± 0.31 µmol-C L^{-1} (n = 38) was also reported on the shelf of the Gulf of Maine (Flores-Cervantes et al., 2009). These limited studies reflect the significant influence of nearby anthropogenic emissions on the abundance of soot in surface waters. Two studies indicate that soot concentration significantly decreases from the shore within a distance of 100 km (Flores-Cervantes et al., 2009; Yang and Guo, 2014). Thus, fluvial discharged soot would mostly settle into sediments close to the shore. In open water, the atmospheric deposition probably determines the abundance of soot in surface oceans. The soot concentrations varied from 0.064 to 0.090 µmol-C L^{-1} below 200 m in the SCS (**Table 1**), which were much higher than 0.005–0.008 µmol-C L^{-1} observed in the mesopelagic water of the northern Gulf of Mexico (Yang and Guo, 2014). Thus, the northern SCS could be characterized as a region with more abundant soot compared with other

open marine environments. The hotspots of BC emissions are expected to be responsible for the higher soot in the SCS. Indeed, the countries rounding the SCS contributed more than one third of the global BC emissions (Bond et al., 2013). Wet precipitation delivers large amounts of BC to the SCS (Mari et al., 2019). In addition, previous studies have shown that the higher DBC concentrations in the upper 100 m of the SCS (avg. 0.97 ± 0.22 μmol-C L^{-1}, $n = 79$) (Fang et al., 2017) compared to those observed in Prydz Bay, Antarctica (0.75 ± 0.26 μmol-C L^{-1}, $n = 17$, Fang et al., 2018) should largely result from enhanced emissions around the SCS.

The vertical distribution of soot, to a certain degree, revealed geochemical processes influencing the cycling of soot in the SCS (**Figure 2A**). In the upper water column, fluctuations in the soot concentration were mainly confined in the upper 50 m (**Figure 2**), probably due to water mixing processes mainly within the mixed layer. This view is further supported by the small variations in the POC_{tot} concentration, TSM concentration, and the soot to POC_{tot} ratio (**Figure 2**). By contrast, the soot exhibited a rapid decrease from 75 to 200 m (**Figure 2A**), potentially due to quick removal *via* photochemical degradation and/or sinking (Stubbins et al., 2012; Feng et al., 2021). This layer, characterized by the steep temperature and salinity gradients as shown in **Figure 1**, largely prevented the vertical mixing of seawater with different soot concentrations. Below the euphotic base, soot concentrations increased with depth like the case of TPM (**Figures 2A,D**). An increase in POC concentration was also observed between 800 and 1,000 m (**Figure 2B**). These results implied additional particulate matter sources in addition to those from the overlying water column. Coppola et al. (2014) suggested that resuspended old sediment BC may contribute to the sinking POC in the North Pacific as supported by the ^{14}C age of BC, highlighting the redistribution mechanism of BC after sedimentation in the ocean. Our recent study indicated that shelf/slope sediments account for 0.22–9.0 g m^{-2} d^{-1} particle fluxes out of the 700–1,000 m in the SCS (Ma et al., 2017). The occurrence of clay minerals in sediment traps and higher diatom flux in the deeper sediment traps also provided evidence for the dispersion of resuspended sediments into the SCS basin (Ran et al., 2015; Schroeder et al., 2015). Mechanistically, internal solitary waves result in the resuspension of the shelf and slope sediments (Zhang et al., 2014; Jia et al., 2019). Then, the resuspended particles lead to higher TPM content in the water column (Zhang et al., 2014) and extra flux below the euphotic zone in the SCS (Lahajnar et al., 2007; Gaye et al., 2009; Liu et al., 2014; Shih et al., 2019). Thus, shelf/slope sediments are also a source of soot in the mesopelagic waters of the northern SCS.

^{210}Po-Derived Export Flux of Soot

Sinking is an important removal pathway of soot from the water column (Flores-Cervantes et al., 2009; Fang et al., 2016). In this study, the disequilibrium between ^{210}Po and ^{210}Pb was used to quantify the sinking flux of soot. The widely used mass-balance model for ^{210}Po (Bacon et al., 1976) was adopted by incorporating advection and diffusion processes. In general, except for upwelling and mesoscale eddy, vertical advection and horizontal diffusion terms are far smaller than vertical

diffusion and horizontal advection (Liang et al., 2014). Thus, we only considered the horizontal advection and vertical diffusion. Briefly, the variation of ^{210}Po with time can be expressed as:

$$\frac{dI_{PoT}}{dt} = \lambda_{Po}\left(I_{PbT} - I_{PoT}\right) + U\frac{\partial I_{PoT}}{\partial x} + k_z\frac{\partial A_{PoT}}{\partial z} - F_{Po} \quad (1)$$

where I_{PoT} and I_{PbT} are the inventories of the total ^{210}Po and ^{210}Pb from surface to the export depth (in dpm m^{-2}). λ_{Po} is the decay constant of ^{210}Po (0.0050 d^{-1}). U and k_z denote the horizontal advection velocity in cm s^{-1} and vertical diffusive coefficient in cm^2 s^{-1}. $\partial I_{PoT}/\partial x$ and $\partial A_{PoT}/\partial z$ represent the gradient of inventory and activity of ^{210}Po, respectively. F_{Po} is the export flux of ^{210}Po (in dpm m^{-2} d^{-1}). At a steady state, the export flux of ^{210}Po becomes:

$$F_{Po} = \lambda_{Po}\left(I_{PbT} - I_{PoT}\right) + U\frac{\partial I_{PoT}}{\partial x} + k_z\frac{\partial A_{PoT}}{\partial z} \quad (2)$$

Due to the lack of horizontal gradient of ^{210}Po in our study, we could not specifically assess the advection flux at the sampling station. However, we used available data collected during August in the north SCS (Ma et al., 2017) to estimate the influence of advection because these data exhibit a similar deficit of ^{210}Po in the mesopelagic SCS. The mean velocities are 15 cm/s in the upper 200 m and 10 cm/s at 500 m during summer in the study area (Gan et al., 2006), where ^{210}Po data have been reported (Ma et al., 2017). The calculated advection fluxes of ^{210}Po account for $17 \pm 21\%$ and $23 \pm 11\%$ of the fluxes at the euphotic base and the mesopelagic bottom, respectively. The estimates indicate that our results ignoring the advection term would, to a certain extent, lead to higher ^{210}Po fluxes at both the euphotic and mesopelagic bases. This overestimate is also propagated to soot flux calculation. In the future, the current-oriented sampling strategy should refine the advection influence. Neglecting advection fluxes will have less of an influence on the application of the soot-^{210}Po coupling to constrain the contribution of soot and POC from the sediments. On the one hand, ^{210}Po fluxes were overestimated by comparable magnitude at the euphotic and mesopelagic bases. Subtracting the advection term largely eliminates the overestimates. On the other hand, the ^{210}Po flux in the mesopelagic water was much higher than 117% (i.e., flux including the influence of advection of 17%) of its flux at the euphotic base. Thus, neglecting advection fluxes will not influence our conclusions. In our study, the vertical gradients of ^{210}Po activity were 0.241 dpm m^{-4} at the euphotic base and 0.009 dpm m^{-4} at the mesopelagic bottom. In the upper SCS, the diffusive coefficient ranges from 10^{-4} to 10^{-5} m^2 s^{-1} even though it could reach 10^{-3} m^2 s^{-1} in the mid-deep water (Wang et al., 2019). Overall, the estimated diffusive fluxes of ^{210}Po account for $<3.1\%$ of the results obtained when neglecting advection and diffusion processes. Thus, the diffusivity of ^{210}Po should not significantly influence our results.

Using the same export model Eq. (2) and also neglecting the advection and diffusion terms, Wei et al. (2014) found that ^{210}Po-derived POC fluxes were comparable to those derived from the floating trap during July–October at the South-East Asian Time-series Study (SEATS) station. The same observations were

also applied to carbonate and particulate nitrogen fluxes (Wei et al., 2014). This comparability lent support to the validity of the $^{210}Po/^{210}Pb$ model in the study area between July and October. In addition, a previous study conducted in our study area that used $^{234}Th/^{238}U$ tracer showed that when considering vertical and horizontal transport in a 3-D model, the results were unreasonable due to poorly constrained model parameters, whereas when using the 1-D Steady State model, such as the one used in this study, they obtained better results (Cai et al., 2015). Thus, we consider that the 1-D $^{210}Po/^{210}Pb$ model is currently the best option to constrain particle dynamics in our study.

The export flux of soot (F_soot) was calculated using F_{Po} multiplied by the soot to $^{210}Po_P$ ratio (in mmol-C dpm^{-1}), i.e.,

$$F\_soot = F_{Po} \times \frac{soot}{Po_P} \qquad (3)$$

where Po_P is the activity concentration of particulate ^{210}Po.

Since ^{210}Po showed deficits with respect to ^{210}Pb from surface to 1,000 m, particles sinking out of the shallow layer are assumed to be responsible for the deficits in deeper layers. Accordingly, the inventories are calculated using trapezoidal integration, with surface and export depths as the upper and lower boundaries. The export flux of soot out of the euphotic zone (at 150 m) was 0.172 ± 0.016 mmol-C m^{-2} d^{-1} (**Table 2**), which is much lower than that of 2.28 mmol-C m^{-2} d^{-1} reported on the shelf of the Gulf of Maine (Flores-Cervantes et al., 2009) and much higher than $0.041–0.097$ mmol-C m^{-2} d^{-1} observed on the Chukchi-Bering Shelf (Fang et al., 2016). Due to the contribution of resuspended sediment from the shelf/slope region to the depth below the euphotic zone, the soot export fluxes were indeed higher than that measured within the euphotic zone, varying from 0.282 ± 0.026 mmol-C m^{-2} d^{-1} to 1.13 ± 0.10 mmol-C m^{-2} d^{-1} (**Figure 3A**).

Below the euphotic zone or in the twilight zone, the soot might experience little photolysis, as was supported by the conservative behavior of DBC in the mesopelagic layer of the SCS (Fang et al., 2017). Thus, soot flux would remain constant in the twilight zone if there is no sediment-derived soot or the sinking velocity of soot is constant. The increase in the concentration of both TPM and soot (**Figure 2**) directly supports the contribution of sediment to the elevated soot flux in the mesopelagic zone at the study site. There is no available sinking velocity of particles in the SCS for assessing its influence on soot flux. The increased sinking velocity of particles with depth was observed in several areas (Villa-Alfageme et al., 2016). If this is true in the study area, the flux of soot (estimated using the velocity multiplied by the concentration) would increase even if the soot concentration does not vary. Thus, the increased soot fluxes in this study may include the effect of the sinking velocity, representing the upper limit of the sediment-contributed soot (i.e., $F\_soot_{sed,i}$), which can be estimated by:

$$F\_soot_{sed,i} = F\_soot_i - F\_soot_{150} \qquad (4)$$

where F_soot_i denotes the total soot flux at a specific depth below 150 m, and $F\text{-}soot_{150}$ is the flux at 150 m, i.e., the euphotic base.

The sediment-derived soot fluxes were estimated to be 0.110 ± 0.030 mmol-C m^{-2} d^{-1} at 200 m, 0.149 ± 0.033 mmol-C m^{-2} d^{-1} at 300 m, and 0.96 ± 0.10 mmol-C m^{-2} d^{-1} at 800 m (**Table 2**). Owing to the sediment addition at different depths (Liu et al., 2014; Jia et al., 2019) and the refractory nature of the soot (Yang and Guo, 2018), the soot flux showed an accumulated effect from the euphotic base to the mesopelagic bottom (**Figure 3B**). In the upper twilight zone (200 and 300 m), sediment contribution accounted for 39–46% of the total soot flux, indicating a significant process for the total soot pool in the SCS interior. Near the mesopelagic bottom at 800 m, sediment-sourced soot accounted for as high as 85% of the total flux. It is obvious that, besides the atmospheric deposition, shelf/slope sediment resuspension is the most relevant process influencing the soot budget in the mesopelagic SCS.

Application of ^{210}Po-Soot Coupling to Constrain Particulate Organic Carbon Export Flux

Particulate organic carbon flux attenuation in the ocean interior is used to constrain the biological pump efficiency at a depth, i.e., the ratio of POC flux at each specific depth in the mesopelagic zone to that at the euphotic zone base (Martin et al., 1987; Buesseler et al., 2007; Chen et al., 2018). In this study, flux attenuation was used to express the variability of local biogenic POC (excluding soot and sediment-derived autochthonous POC) flux with depth in the study area. Appling Eq. (3) using the POC/Po_P ratios measured on bottle-sampled TPM, the export fluxes of POC_{tot} were estimated (**Figure 3C**). The $POC_{tot}/^{210}Po_P$ ratio for bottle-sampled TPM was comparable to that of the sediment-trap sample below the euphotic zone (i.e., 200 m), though a little difference was observed at 50 m (**Figure 4**). Due to the lack of trap sample at most depths, the POC/Po_P ratios on bottle-sampled TPM were thus used to calculate the fluxes of POC to facilitate the comparison of POC fluxes at different depths. The POC_{tot} varied from 5.44 ± 0.49 mmol-C m^{-2} d^{-1} to 33.6 ± 2.9 mmol-C m^{-2} d^{-1} (**Table 2**), averaging 12.3 mmol-C m^{-2} d^{-1}. Notably, the POC_{tot} flux at 200 m was about four times that at 50 m (**Figure 4**), corresponding to the higher primary productivity in the lower euphotic zone than the upper euphotic zone (Cai et al., 2015).

Since the soot is mostly of terrestrial origin (Gustafsson et al., 2001; Yang and Guo, 2018), the autochthonous POC (POC_{auto}) includes $POC_{auto,loc}$ from the local euphotic zone and $POC_{auto,sed}$ from the sediment, but excludes the soot. The calculated POC_{auto} fluxes ranged from 5.12 ± 0.46 mmol-C m^{-2} d^{-1} to 10.49 ± 0.94 mmol-C m^{-2} d^{-1} (**Table 2**). In addition, the $POC_{auto,loc}$ flux out of the euphotic zone (5.97 ± 0.55 mmol-C m^{-2} d^{-1}) was comparable to 4.0 ± 1.6 mmol-C m^{-2} d^{-1} ($n = 10$) previously reported for the adjacent region in the same season (Cai et al., 2015), also supporting the validity of the $^{210}Po/^{210}Pb$ model.

Below the euphotic base, the POC_{auto} flux showed an increasing trend as observed for the flux of soot (**Figure 3D**). Obviously, the shelf/slope sediment contributed POC_{auto} to the mesopelagic SCS. Based on the fact that $POC_{auto,sed}$ and soot were

TABLE 2 | The export fluxes of total POC (F_POC_{tot}) and soot ($F\text{-soot}$), autochthonous POC (i.e., soot-excluded POC, F_POC_{auto}), sediment contributed soot flux (F_soot_{sed}) and autochthonous POC ($F\_POC_{auto,sed}$), and autochthonous POC contributed by local ecosystems in the euphotic zone ($F\_POC_{auto,loc}$).

Depth	F_soot	F_soot_{sed}	F_POC_{tot}	F_POC_{auto}	$F\_POC_{auto,sed}$	$F\_POC_{auto,loc}$
(m)	(mmol-C m^{-2} d^{-1})					
150	0.172 ± 0.016		6.14 ± 0.56	5.97 ± 0.55		5.97 ± 0.55
200	0.282 ± 0.026	0.110 ± 0.030	6.20 ± 0.57	5.92 ± 0.54	0.99 ± 0.27	4.93 ± 0.54
300	0.322 ± 0.029	0.149 ± 0.033	5.44 ± 0.49	5.12 ± 0.46	1.34 ± 0.30	3.78 ± 0.53
500			10.7 ± 1.0			
800	1.13 ± 0.10	0.96 ± 0.10	11.6 ± 1.0	10.49 ± 0.94	8.63 ± 0.93	1.87 ± 0.94
1000			33.6 ± 2.9			

These fluxes were estimated based on the ratios of POC or soot contents to ^{210}Po activities on total particulate matter (TPM) collected from the water column.
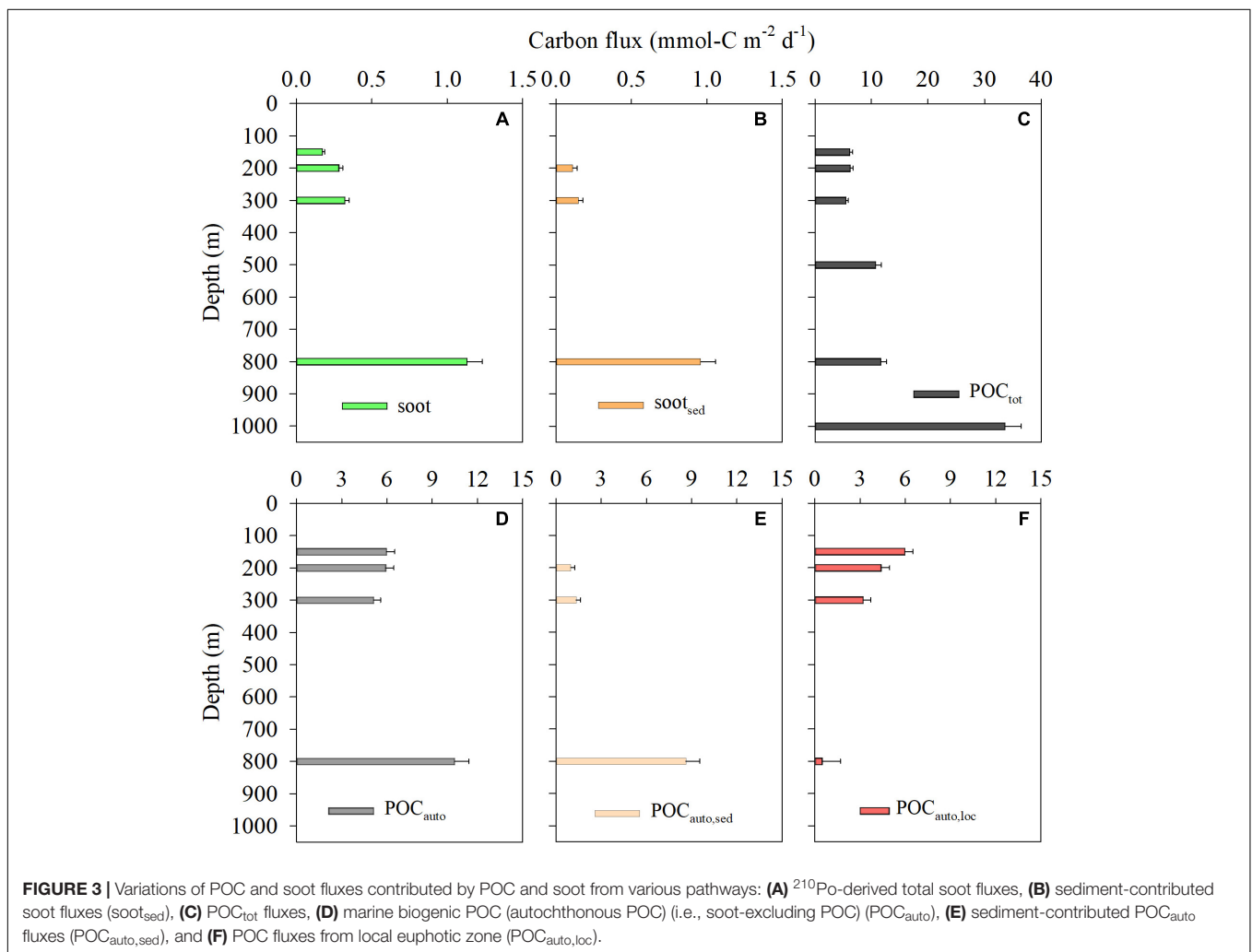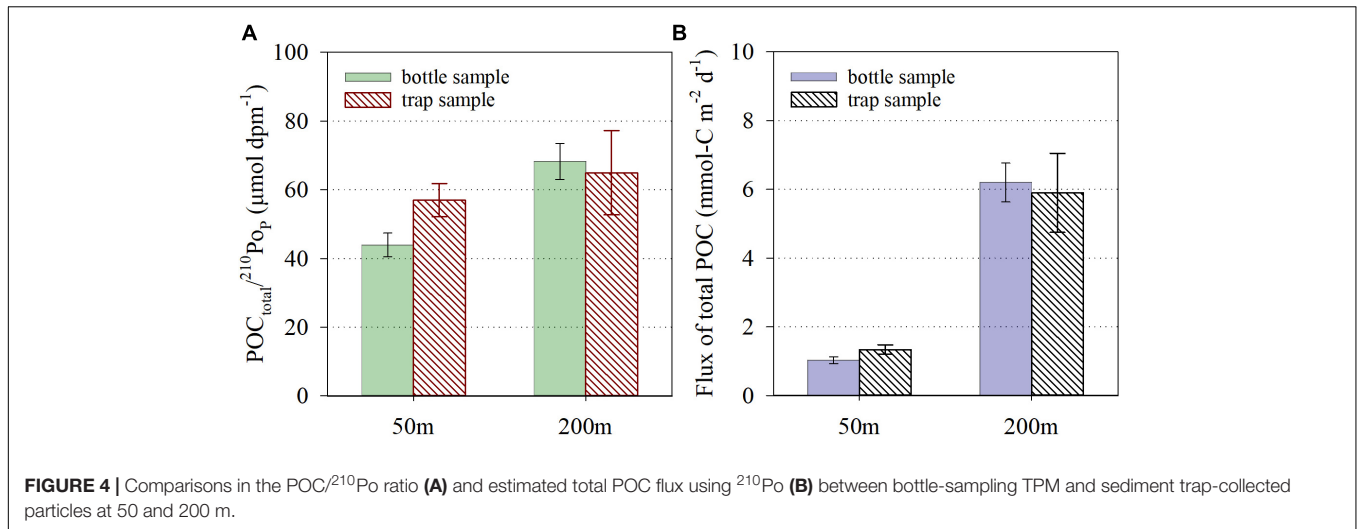

FIGURE 3 | Variations of POC and soot fluxes contributed by POC and soot from various pathways: **(A)** ^{210}Po-derived total soot fluxes, **(B)** sediment-contributed soot fluxes (soot$_{sed}$), **(C)** POC$_{tot}$ fluxes, **(D)** marine biogenic POC (autochthonous POC) (i.e., soot-excluding POC) (POC$_{auto}$), **(E)** sediment-contributed POC$_{auto}$ fluxes (POC$_{auto,sed}$), and **(F)** POC fluxes from local euphotic zone (POC$_{auto,loc}$).

concurrently resuspended, the ^{210}Po-derived F_soot_{sed} and the SOC/soot ratio in surface sediments were used to estimate the POC$_{auto,sed}$ contribution to POC$_{auto}$ flux, i.e.,

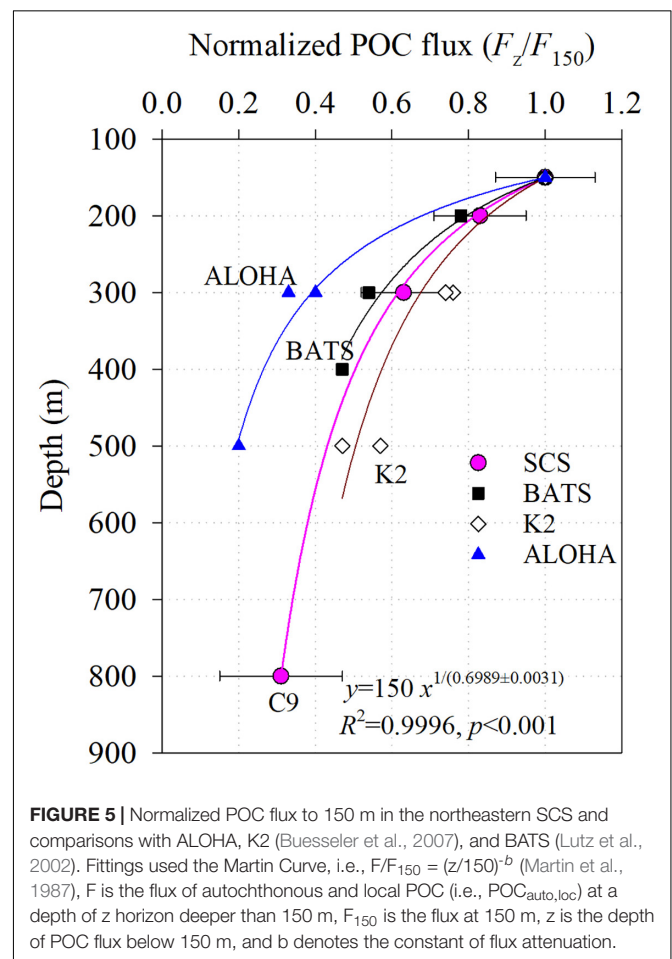$$F\_POC_{auto,sed,i} = F\_soot_{sed,i} \times \frac{SOC}{soot} \qquad (5)$$

where $F\_POC_{auto,sed,i}$ and $F\_soot_{sed,i}$ denote the fluxes of $F\_POC_{auto,sed}$ and F_soot_{sed} at the specific i depth, respectively.

SOC/soot is the ratio of the content of SOC to that of soot in surface sediments. At the two locations where sediment samples were collected (**Figure 1**), the SOC/soot ratio in surface sediments varied from 9.8 to 10.3%. Here, 10% was adopted for estimating the POC$_{auto,sed}$ contribution. It should be noted that the SOC/soot ratio may be different at different shelf/slope sites, and further measurements are needed to confirm this ratio in other regions.

FIGURE 4 | Comparisons in the POC/^{210}Po ratio **(A)** and estimated total POC flux using ^{210}Po **(B)** between bottle-sampling TPM and sediment trap-collected particles at 50 and 200 m.

Based on Eq. (5), the POC$_{auto,sed}$ fluxes were estimated to be 0.99 ± 0.27 mmol-C m^{-2} d^{-1} at 200 m, 1.34 ± 0.30 mmol-C m^{-2} d^{-1} at 300 m, and 8.63 ± 0.93 mmol-C m^{-2} d^{-1} at 800 m (**Table 2** and **Figure 3E**). Thus, the POC$_{auto,loc}$ fluxes in the mesopelagic waters can be calculated by subtracting the POC$_{auto,sed}$ fluxes from the POC$_{auto}$ fluxes. The POC$_{auto,loc}$ flux decreased from 4.93 ± 0.54 mmol-C m^{-2} d^{-1} at 200 m to 1.87 ± 0.94 mmol-C m^{-2} d^{-1} at 800 m, showing an attenuation from the euphotic base to 800 m like observations in open oceans (**Figure 3F**).

With the separation of POC$_{auto,loc}$ from POC$_{auto,sed}$, the first vertical distribution of $F\_POC_{auto,loc}$ in the SCS was used to compare the biological pump efficiency between the SCS and other oceanic settings. In the open ocean, the downward flux attenuation of POC is commonly described by the Martin Curve, i.e., $F_z/F_{z0} = (z/z_0)^{-b}$ (Martin et al., 1987), where b describes the flux attenuation rate. The Martin Curve simulates the profiles of POC flux in the water column, and it has been widely used to evaluate the variability of POC fluxes from the euphotic zone to the deep ocean. By normalizing our ^{210}Po-soot-based $F\_POC_{auto,loc}$ to that at 150 m, b is 0.70 ± 0.01 ($R^2 = 0.9996$, $p < 0.001$) (**Figure 5**). Martin et al. (1987) first reported b values ranging from 0.64 to 0.97 in the Pacific. Later, 1.33 ± 0.15 and 0.51 ± 0.05 were reported for ALOHA and K2 stations (from the VERTIGO project) (**Figure 5**; Buesseler et al., 2007). At station BATS (online data and Lutz et al., 2002), b was 0.83 ± 0.04 (**Figure 5**) and the global mean value was 0.9–1.0 (Kwon et al., 2009). Our result observed in the oligotrophic SCS is comparable to that at station BATS. Globally, the SCS showed a low-moderate attenuation coefficient. Previous studies suggested that particle sinking velocity and temperature mainly influence the transport of POC to mesopelagic water (Buesseler et al., 2007; Henson et al., 2015; Le Moigne et al., 2016). Villa-Alfageme et al. (2016) reported valuable average sinking velocities (ASVs) of TPM at station BATS, showing an increase with depth. Considering the similar oligotrophic environments between the SCS and BATS, it is probable that high temperatures in the euphotic zone in the SCS (e.g., > 20°C in the upper 100 m, **Figure 1**) benefits the

FIGURE 5 | Normalized POC flux to 150 m in the northeastern SCS and comparisons with ALOHA, K2 (Buesseler et al., 2007), and BATS (Lutz et al., 2002). Fittings used the Martin Curve, i.e., F/F$_{150}$ = (z/150)$^{-b}$ (Martin et al., 1987), F is the flux of autochthonous and local POC (i.e., POC$_{auto,loc}$) at a depth of z horizon deeper than 150 m, F$_{150}$ is the flux at 150 m, z is the depth of POC flux below 150 m, and b denotes the constant of flux attenuation.

fast remineralization of slow-sinking particles in shallow water, allowing faster-sinking particles to reach the mesopelagic zone, as observed at BATS (Villa-Alfageme et al., 2016). Owing to limited studies on POC transport in the mesopelagic water in

the SCS, extensive studies are needed to elucidate the mechanism controlling the biological pump in the mesopelagic zone of the SCS. Overall, our study indicated that ^{210}Po-soot coupling could provide insights into the POC flux in the mesopelagic zone.

CONCLUDING REMARKS

The abundance and export of soot were first evaluated in the northeastern SCS. The results indicated that several processes affected the geochemical cycling of soot in the marine environment. In the surface mixed layer, water mixing played a predominant role in determining the vertical distribution of soot, showing a homogenized soot concentration. In the lower euphotic zone with steep temperature and salinity gradients, photodegradation processes dominated, resulting in a decrease in soot concentrations with depth until the base of the euphotic zone. Below the euphotic zone, sediment resuspension in the shelf/slope region and lateral transport contributed to the increase in soot abundance and fluxes in the mesopelagic layer. The refractory nature of soot lends support for distinguishing the local soot sinking-flux from the sediment-derived soot flux in the twilight zone. By utilizing soot (terrestrial and bio-resistant in nature) and ^{210}Po-derived POC flux, the local sinking POC flux from the overlying euphotic zone can be separated from the sediment-derived POC. These results revealed the potential application of ^{210}Po-soot coupling to constrain POC fluxes in marginal seas.

REFERENCES

Bacon, M. P., Spencer, D. W., and Brewer, P. G. (1976). ^{210}Pb/^{226}Ra and ^{210}Po/^{210}Pb disequilibria in seawater and suspended particulate matter. *Earth Planet. Sci. Lett.* 32, 277–296. doi: 10.1016/0012-821X(76)90068-6

Bao, H., Niggemann, J., Luo, L., Dittmar, T., and Kao, S.-J. (2017). Aerosols as a source of dissolved black carbon to the ocean. *Nat. Commun.* 8:510. doi: 10.1038/s41467-017-00437-3

Bond, T. C., Doherty, S. J., Fahey, D. W., Forster, P. M., Berntsen, T., DeAngelo, B. J., et al. (2013). Bounding the role of black carbon in the climate system: a scientific assessment. *J. Geophys. Res. Atmos.* 118, 5380–5552. doi: 10.1002/jgrd.50171

Buesseler, K. O., Lamborg, C. H., Boyd, P. W., Lam, P. J., Trull, T. W., Bidigare, R. R., et al. (2007). Revisiting carbon flux through the ocean's twilight zone. *Science* 316, 567–570. doi: 10.1126/science.1137959

Cai, P., Zhao, D., Wang, L., Huang, B., and Dai, M. (2015). Role of particle stock and phytoplankton community structure in regulating particulate organic carbon export in a large marginal sea. *J. Geophys. Res. Oceans* 120, 2063–2095. doi: 10.1002/2014JC010432

Chen, C.-T. A., Wang, S.-L., Wang, B.-J., and Pai, S.-C. (2001). Nutrient budgets for the South China Sea basin. *Mar. Chem.* 75, 281–300. doi: 10.1016/S0304-4203(01)00041-X

Chen, Y., Wu, Z., and Li, Q. (2018). Temporal change of export production at Xisha of the Northern South China Sea. *J. Geophys. Res. Oceans* 123, 9305–9319. doi: 10.1029/2017JC013619

Cheng, C.-H., Lehmann, J., and Engelhard, M. H. (2008). Natural oxidation of black carbon in soils: changes in molecular form and surface charge along a climosequence. *Geochim. Cosmochim. Acta* 72, 1598–1610. doi: 10.1016/j.gca.2008.01.010

Church, T. M., Rigaud, S., Baskaran, M., Kumar, A., Friedrich, J., Masqué, P., et al. (2012). Intercalibration studies of ^{210}Po and ^{210}Pb in dissolved and particulate seawater samples. *Limnol. Oceanogr. Methods* 10, 776–789. doi: 10.4319/lom.2012.10.776

Coppola, A. I., and Druffel, E. R. M. (2016). Cycling of black carbon in the ocean. *Geophys. Res. Lett.* 43, 4477–4482. doi: 10.1002/2016GL068574

Coppola, A. I., Wiedemeier, D. B., Galy, V., Haghipour, N., Hanke, U. M., Nascimento, G. S., et al. (2018). Global-scale evidence for the refractory nature of riverine black carbon. *Nat. Geosci.* 11, 584–588. doi: 10.1038/s41561-018-0159-8

Coppola, A. I., Ziolkowski, L. A., Masiello, C. A., and Druffel, E. R. M. (2014). Aged black carbon in marine sediments and sinking particles. *Geophys. Res. Lett.* 41, 2427–2433. doi: 10.1002/2013GL059068

Dittmar, T., Eduardo de Rezende, C., Manecki, M., Niggemann, J., Ovalle, A. R. C., Stubbins, A., et al. (2012). Continuous flux of dissolved black carbon from a vanished tropical forest biome. *Nat. Geosci.* 5, 618–622. doi: 10.1038/ngeo1541

Elmquist, M., Gustafsson, Ö, and Andersson, P. (2004). Quantification of sedimentary black carbon using the chemothermal oxidation method: an evaluation of ex situ pre-treatments and standard additions approaches. *Limnol. Oceanogr. Methods* 2, 417–427. doi: 10.4319/lom.2004.2.417

Fang, Z., Yang, W., Chen, M., and Ma, H. (2017). Source and fate of dissolved black carbon in the western South China Sea during the Southwest Monsoon prevailing season. *J. Geophys. Res. Biogeosci.* 122, 2817–2830. doi: 10.1002/2017JG004014

Fang, Z., Yang, W., Chen, M., Stubbins, A., Ma, H., and Jia, R. (2018). Transport of dissolved black carbon from the Prydz Bay Shelf, Antarctica to the deep Southern Ocean. *Limnol. Oceanogr.* 63, 2179–2190. doi: 10.1002/lno.10932

Fang, Z., Yang, W., Chen, M., Zheng, M., and Hu, W. (2016). Abundance and sinking of particulate black carbon in the western Arctic and Subarctic Oceans. *Sci. Rep.* 6:29959. doi: 10.1038/srep29959

Fang, Z., Yang, W., Stubbins, A., Chen, M., Li, J., Jia, R., et al. (2021). Spatial characteristics and removal of dissolved black carbon in the western Arctic Ocean and Bering Sea. *Geochim. Cosmochim. Acta* 304, 178–190. doi: 10.1016/j.gca.2021.04.024

Feng, N., Yang, W., Zhao, X., Chen, M., Qiu, Y., and Zheng, M. (2021). Semi-enclosed bays server as hotspots for black carbon burial: a case study in Jiaozhou Bay, western Yellow Sea. *Sci. Total Environ.* 797:149100. doi: 10.1016/j.scitotenv.2021.149100

Flores-Cervantes, D. X., Plata, D. L., MacFarlane, J. K., Reddy, C. M., and Gschwend, P. M. (2009). Black carbon in marine particulate organic carbon: inputs and cycling of highly recalcitrant organic carbon in the Gulf of Maine. *Mar. Chem.* 113, 172–181. doi: 10.1016/j.marchem.2009.01.012

Gan, J., Li, H., Curchitser, E. N., and Haidvogel, D. B. (2006). Modeling South China Sea circulation: response to seasonal forcing regimes. *J. Geophys. Res.* 111:C06034. doi: 10.1029/2005JC003298

Gaye, B., Wiesner, M. G., and Lahajnar, N. (2009). Nitrogen sources in the South China Sea, as discerned from stable nitrogen isotopic ratios in rivers, sinking particles, and sediments. *Mar. Chem.* 114, 72–85. doi: 10.1016/j.marchem.2009.04.003

Goldberg, E. D. (1985). *Black Carbon In The Environment*. New York: John Wiley.

Gustafsson, Ö, Bucheli, T. D., Kukulska, Z., Andersson, M., Largeau, C., Rouzaud, J.-N., et al. (2001). Evaluation of a protocol for the quantification of black carbon in sediments. *Glob. Biogeochem. Cycles* 15, 881–890. doi: 10.1029/2000GB001380

Gustafsson, Ö, Haghseta, F., Chan, C., Macfarlane, J., and Gschwend, P. M. (1997). Quantification of the dilute sedimentary soot phase: implications for PAH speciation and bioavailability. *Environ. Sci. Technol.* 31, 203–209. doi: 10.1021/es960317s

Henson, S. A., Yool, A., and Sanders, R. J. (2015). Variability in efficiency of particulate organic carbon export: a model study. *Glob. Biogeochem. Cycles* 29, 33–45. doi: 10.1002/2014GB004965

Hu, L., Shi, X., Bai, Y., Fang, Y., Chen, Y., Qiao, S., et al. (2016). Distribution, input pathway and mass inventory of black carbon in sediments of the Gulf of Thailand, SE Asia. *Estuar. Cost. Shelf Sci.* 170, 10–19. doi: 10.1016/j.ecss.2015.12.019

Jacobson, M. Z. (2001). Strong radiative heating due to the mixing state of black carbon in atmospheric aerosols. *Nature* 409, 695–697. doi: 10.1038/35055518

Jia, Y., Tian, Z., Shi, X., Liu, J. P., Chen, J., and Liu, X. (2019). Deep-sea sediment resuspension by internal solitary waves in the Northern South China Sea. *Sci. Rep.* 9:12137. doi: 10.1038/s41598-019-47886-y

Jones, M. W., Coppola, A. I., Santín, C., Dittmar, T., Jaffé, R., Doerr, S. H., et al. (2020). Fires prime terrestrial organic carbon for riverine export to the global oceans. *Nat. Commun.* 11:2791. doi: 10.1038/s41467-020-16576-z

Jurado, E., Dashs, J., Duarte, C. M., and Simó, R. (2008). Atmospheric deposition of organic and black carbon. *Atmos. Environ.* 42, 7931–7939. doi: 10.1016/j.atmosenv.2008.07.029

Kwon, E. Y., Primeau, F., and Sarmiento, J. L. (2009). The impact of remineralization depth on the air-sea carbon balance. *Nat. Geosci.* 2, 630–635. doi: 10.1038/ngeo612

Lahajnar, N., Wiesner, M. G., and Gaye, B. (2007). Fluxes of amino acids and hexosamines to the deep South China Sea. *Deep Sea Res. I* 54, 2120–2144. doi: 10.1016/j.dsr.2007.08.009

Le Moigne, F. A. C., Henson, S. A., Cavan, E., Georges, C., Pabortsava, K., Achterberg, E. P., et al. (2016). What causes the inverse relationship between primary production and export efficiency in the Southern Ocean?. *Geophys. Res. Lett.* 43, 4457–4466. doi: 10.1002/2016GL068480

Liang, H., Zhao, W., Dai, D., and Zhang, J. (2014). Estimation of vertical diffusion coefficient based on a onedimensional temperature diffusion equation with an inverse method. *Acta Oceanol. Sin.* 33, 28–36. doi: 10.1007/s13131-014-0472-z

Liu, J., Clift, P. D., Yan, W., Chen, Z., Chen, H., Xiang, R., et al. (2014). Modern transport and deposition of settling particles in the northern South China Sea: sediment trap evidence adjacent to Xisha Trough. *Deep Sea Res. I* 93, 145–155. doi: 10.1016/j.dsr.2014.08.005

Lohmann, R., Bollinger, K., Cantwell, M., Feichter, J., Fischer-Bruns, I., and Zabel, M. (2009). Fluxes of soot black carbon to South Atlantic sediments. *Glob. Biogeochem. Cycles* 23:GB1015. doi: 10.1029/2008GB003253

Louchouarn, P., Chillrud, R. N., Houel, S., Yan, B., Chaky, D., Rumpel, C., et al. (2007). Elemental and molecular evidence of soot-and char-derived black carbon inputs to New York City's atmosphere during the 20th century. *Environ. Sci. Technol.* 41, 82–87. doi: 10.1021/es061304+

Lutz, M., Dunbar, R., and Caldeira, K. (2002). Regional variability in the vertical flux of particulate organic carbon in the ocean interior. *Glob. Biogeochem. Cycles* 16:1037. doi: 10.1029/2000GB001383

Ma, H., Yang, W., Zhang, L., Zhang, R., Chen, M., Qiu, Y., et al. (2017). Utilizing ^{210}Po deficit to constrain particle dynamics in mesopelagic water, western South China Sea. *Geochem. Geophys. Geosys.* 18, 1594–1607. doi: 10.1002/2017GC006899

Mari, X., Guinot, B., Thuoc, C. V., Brune, J., Lefebvre, J.-P., Sriram, P. R. A., et al. (2019). Biogeochemical impacts of a black carbon wet deposition event in Halong Bay, Vietnam. *Front. Mar. Sci.* 6:185. doi: 10.3389/fmars.2019.00185

Martin, J. H., Knauer, G. A., Karl, D. M., and Broenkow, W. W. (1987). VERTEX: carbon cycling in the northeast Pacific. *Deep Sea Res. A* 34, 267–285. doi: 10.1016/0198-0149(87)90086-0

Masiello, C. A., and Druffel, E. R. M. (1998). Black carbon in deep-sea sediments. *Science* 280, 1911–1913. doi: 10.1126/science.280.5371.1911

Qi, Y., Fu, W., Tian, J., Luo, C., Shan, S., and Sun, S. (2020). Dissolved black carbon is not likely a significant refractory organic carbon pool in rivers and oceans. *Nat. Commun.* 11:5051. doi: 10.1038/s41467-020-18808-8

Ramanathan, V., and Carmichael, G. (2008). Global and regional climate changes due to black carbon. *Nat. Geosci.* 1, 221–227. doi: 10.1038/ngeo156

Ran, L., Chen, J., Wiesner, M. G., Ling, Z., Lahajnar, N., Yang, Z., et al. (2015). Variability in the abundance and species composition of diatoms in sinking particles in the northern South China Sea: results from time-series moored sediment traps. *Deep Sea Res. II* 122, 15–24. doi: 10.1016/j.dsr2.2015.07.004

Rigaud, S., Puigorbé, V., Camara-Mor, P., Casacuberta, N., Roca-Martí, M., Garcia-Orellana, J., et al. (2013). A methods assessment and recommendations for improving calculations and reducing uncertainties in the determination of ^{210}Po and ^{210}Pb activities in seawater. *Limnol. Oceanogr. Methods* 11, 561–571. doi: 10.4319/lom.2013.11.561

Roca-Martí, M., Puigcorbé, V., Castrillejo, M., Casacuberta, N., Garcia-Orellana, J., Cochran, J. K., et al. (2021). Quantifying ^{210}Po/^{210}Pb disequilibrium in seawater: a comparison of two precipitation methods with differing results. *Front. Mar. Sci.* 8:684484. doi: 10.3389/fmars.2021.684484

Schroeder, A., Wiesner, M. G., and Liu, Z. (2015). Fluxes of clay minerals in the South China Sea. *Earth Planet. Sci. Lett.* 430, 30–42. doi: 10.1016/j.epsl.2015.08.001

Shih, Y.-Y., Lin, H.-H., Li, D., Hsieh, H.-H., Hung, C.-C., and Chen, C.-T. A. (2019). Elevated carbon flux in deep waters of the South China Sea. *Sci. Rep.* 9:1496. doi: 10.1038/s41598-018-37726-w

Singh, N., Abiven, S., Torn, M. S., and Schmidt, M. W. I. (2012). Fire-derived organic carbon in soil turns over on a centennial scale. *Biogeosciences* 9, 2847–2857. doi: 10.5194/bg-9-2847-2012

Stubbins, A., Niggemann, J., and Dittmar, T. (2012). Photo-lability of deep ocean dissolved black carbon. *Biogeosciences* 9, 1661–1670. doi: 10.5194/bg-9-1661-2012

Villa-Alfageme, M., de Soto, F. C., Ceballos, E., Giering, S. L. C., Le Moigne, F. A. C., Henson, S., et al. (2016). Geographical, seasonal, and depth variation in sinking particle speeds in the North Atlantic. *Geophys. Res. Lett.* 43, 8609–8616. doi: 10.1002/2016GL069233

Wagner, S., Brandes, J., Spencer, R. G. M., Ma, K., Rosengard, S. Z., Moura, J. M. S., et al. (2019). Isotopic composition of oceanic dissolved black carbon reveals non-riverine source. *Nat. Commun.* 10:5064. doi: 10.1038/s41467-019-13111-7

Wagner, S., Jaffé, R., and Stubbins, A. (2018). Dissolved black carbon in aquatic ecosystems. *Limnol. Oceanogr. Lett.* 3, 168–185. doi: 10.1002/lol2.10076

Wang, D., Wang, Q., Cai, S., Shang, X., Peng, S., Shu, Y., et al. (2019). Advances in research of the mid-deep South China Sea circulation. *Sci. China Earth Sci.* 62, 1992–2004. doi: 10.1007/s11430-019-9546-3

Wang, X., Xu, C., Druffel, E. M., Xue, Y., and Qi, Y. (2016). Two black carbon pools transported by the Changjiang and Huanghe Rivers in China. *Glob. Biogeochem. Cycles* 30, 1778–1790. doi: 10.1002/2016GB005509

Wang, Z., Yang, W., Chen, M., Lin, P., and Qiu, Y. (2014). Intra-annual deposition of atmospheric ^{210}Pb, ^{210}Po and the residence times of aerosol in Xiamen, China. *Aerosol Air Qual. Res.* 14, 1402–1410. doi: 10.4209/aaqr.2013.05.0170

Ward, C. P., Sleighter, R. L., Hatcher, P. G., and Cory, R. M. (2014). Insights into the complete and partial photooxidation of black carbon in surface waters. *Environ. Sci. Process. Impacts* 16, 721–731. doi: 10.1039/c3em00597f

Wei, C.-L., Lin, S.-Y., Sheu, D. D., Chou, W.-C., Yi, M.-C., Santschi, P. H., et al. (2011). Particle-reactive radionuclides (^{234}Th, ^{210}Pb, ^{210}Po) as tracers for the estimation of export production in the South China Sea. *Biogeosciences* 8, 3793–3808. doi: 10.5194/bg-8-3793-2011

Wei, C.-L., Yi, M.-C., Lin, S.-Y., Wen, L.-S., and Lee, W.-H. (2014). Seasonal distributions and fluxes of ^{210}Pb and ^{210}Po in the northern South China Sea. *Biogeosciences* 11:6813v6826. doi: 10.5194/bg-11-6813-2014

Yang, W., and Guo, L. (2014). Abundance, distribution and isotopic composition of particulate black carbon in the northern Gulf of Mexico. *Geophys. Res. Lett.* 41, 7619–7625. doi: 10.1002/2014GL061912

Yang, W., and Guo, L. (2018). Sources and burial fluxes of soot black carbon in sediments on the Mackenzie, Chukchi, and Bering Shelves. *Cont. Shelf Res.* 155, 1–10. doi: 10.1016/j.csr.2018.01.008

Yang, W., Guo, L., Chuang, C. Y., Schumann, D., Ayranov, M., and Santschi, P. H. (2013). Adsorption characteristics of ^{210}Pb, ^{210}Po and ^{7}Be onto micro-particle surfaces and the effects of macromolecular organic compounds. *Geochim. Cosmochim. Acta* 107, 47–64. doi: 10.1016/j.gca.2012.12.039

Yang, W., Huang, Y., Chen, M., Qiu, Y., Peng, A., and Zhang, L. (2009). Export and remineralization of POM in the Southern Ocean and the South China Sea estimated from ^{210}Po/^{210}Pb disequilibria. *Chin. Sci. Bull.* 54, 2118–2123. doi: 10.1007/s11434-009-0043-4

Zhang, J., Li, H., Xuan, J., Wu, Z., Yang, Z., Wiesner, M. G., et al. (2019). Enhancement of mesopelagic sinking particle fluxes due to upwelling, aerosol deposition, and monsoonal influences in the northwestern South China Sea. *J. Geophys. Res. Oceans* 124, 99–112. doi: 10.1029/2018JC014704

Zhang, L., Yang, W., Chen, M., Wang, Z., Lin, P., Fang, Z., et al. (2016). Atmospheric deposition of ^{7}Be in the southeast of China: a case study in Xiamen. *Aerosol Air Qual. Res.* 16, 105–113. doi: 10.4209/aaqr.2015.03.0182

Zhang, X., Chen, J., Xiang, L., Fang, J., Li, Y., Zhu, Y., et al. (2014). A preliminary study on the characteristics of marine nepheloid layers in the northern South China Sea and their influential factors. *Acta Oceanol. Sin.* 36, 51–65.

Ziolkowski, L. A., and Druffel, E. R. M. (2010). Aged black carbon identified in marine dissolved organic carbon. *Geophys. Res. Lett.* 37:L16601. doi: 10.1029/2010GL043963